

Electronic Supplementary Information (ESI)

**Ni₃Fe/Ni₃Fe(OOH)_x Dynamically Coupled on Wood-Derived Nitrogen-Doped Carbon as
Bifunctional Electrocatalyst for Rechargeable Zinc-Air Batteries**

Yi Wang^a, Yanyan Liu^{a,b,c*}, Limin Zhou^a, Pengxiang Zhang^a, Xianli Wu^a, Tao Liu^{a,d}, Sehrish Mehdi^{a,e}, Xianji Guo^{a*}, Jianchun Jiang^c and Baojun Li^{a,c}

^a College of Chemistry, Zhengzhou University, 100 science road, Zhengzhou 450001, P. R. China.

^b College of Science, Henan Agricultural University, 63 Agriculture Road, Zhengzhou 450002, P.R. China.

^c Institute of Chemistry Industry of Forest Products, CAF, National Engineering Lab for Biomass Chemical Utilization, 16 Suojinwucun, Nanjing 210042, P. R. China.

^d CAS Key Laboratory for Biomedical Effects of Nanomaterials and Nanosafety, National Center for Nanoscience and Technology, Beijing 100190, P.R. China.

^e Department of Chemistry, The Women University, Kutchery Campus, L.M.Q. Road, Multan, 66000, Pakistan.

* Corresponding Author. E-mail: lyylhs180208@163.com (Y. Y. Liu) and guoxj@zzu.edu.cn (X.J. Guo).

Total number of pages: 24

Total number of figures: 17

Total number of tables: 8

Table of Contents

Experimental Section.....	S3
Figure S1.....	S4
Figure S2.....	S5
Figure S3.....	S6
Figure S4.....	S7
Figure S5.....	S8
Figure S6.....	S9
Figure S7.....	S10
Figure S8.....	S10
Figure S9.....	S10
Figure S10.....	S11
Figure S11.....	S11
Figure S12.....	S12
Figure S13.....	S12
Figure S14.....	S12
Figure S15.....	S13
Figure S16.....	S14
Figure S17.....	S14
Table S1.....	S15
Table S2.....	S16
Table S3.....	S17
Table S4.....	S18
Table S5.....	S19
Table S6.....	S20
Table S7.....	S21
Table S8.....	S22
References.....	S23

Experimental Section

The detail of DFT calculations

We have employed the first-principles to perform all Spin-polarization density functional theory (DFT) calculations within the generalized gradient approximation (GGA) using the Perdew-Burke-Ernzerhof (PBE) formulation. We have chosen the projected augmented wave (PAW) potentials to describe the ionic cores and take valence electrons into account using a plane wave basis set with a kinetic energy cutoff of 520 eV. Partial occupancies of the Kohn-Sham orbitals were allowed using the Gaussian smearing method and a width of 0.05 eV. The electronic energy was considered self-consistent when the energy change was smaller than 10^{-5} eV. A geometry optimization was considered convergent when the energy change was smaller than 0.05 eV Å⁻¹. In our structure, the U correction is used for Ni and Fe atoms. The vacuum spacing in a direction perpendicular to the plane of the structure is 20 Å for the structures. The Brillouin zone integration is performed using 2×2×1 Monkhorst-Pack k-point sampling for a structure. Finally, the adsorption energies(E_{ads}) were calculated as $E_{\text{ads}} = E_{\text{ad/sub}} - E_{\text{ad}} - E_{\text{sub}}$, where $E_{\text{ad/sub}}$, E_{ad} , and E_{sub} are the total energies of the optimized adsorbate/substrate system, the adsorbate in the structure, and the clean substrate, respectively. The free energy was calculated using the equation:

$$G = E_{\text{ads}} + ZPE - TS \quad (4)$$

The G , E_{ads} , ZPE and TS are the free energy, total energy from DFT calculations, zero point energy and entropic contributions, respectively.

Supplementary Figures

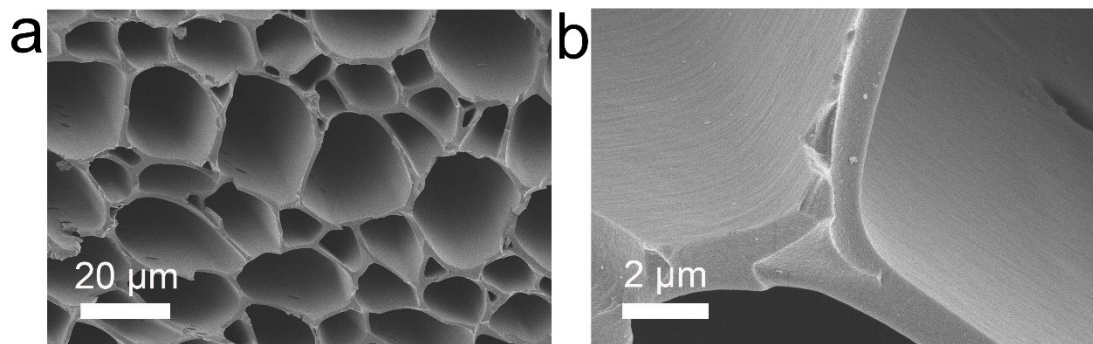


Fig. S1. SEM images of (a, b) NWC.

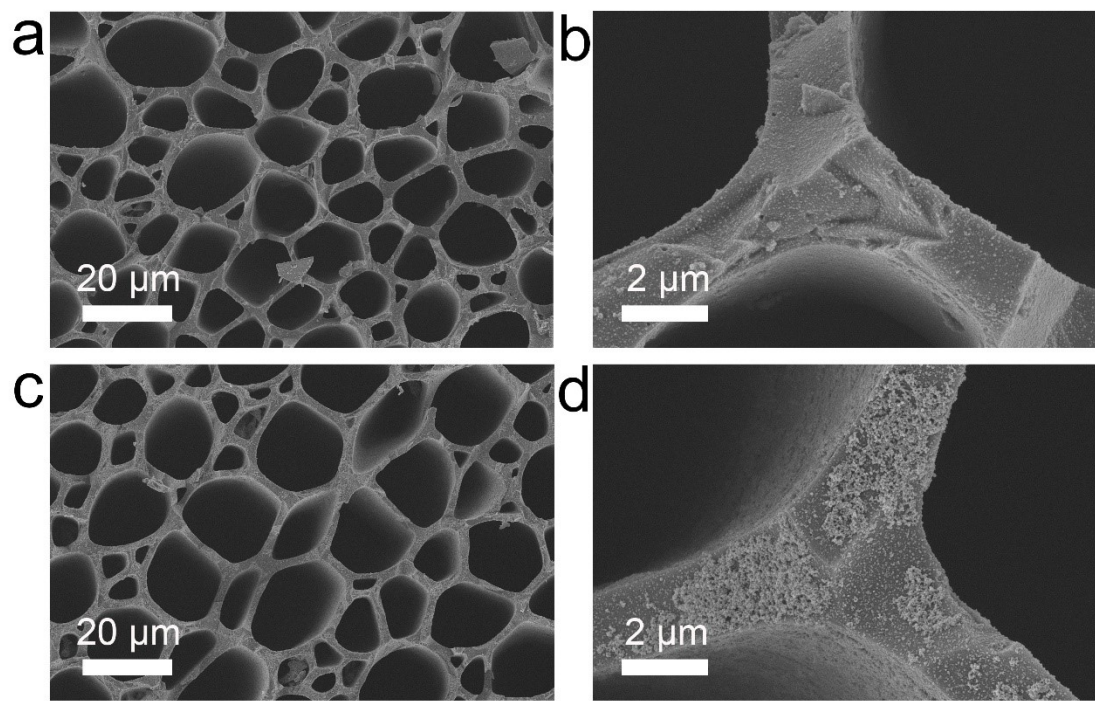


Fig. S2. SEM images of (a, b) Fe-OH@NWC, and (c, d) Fe@NWC.

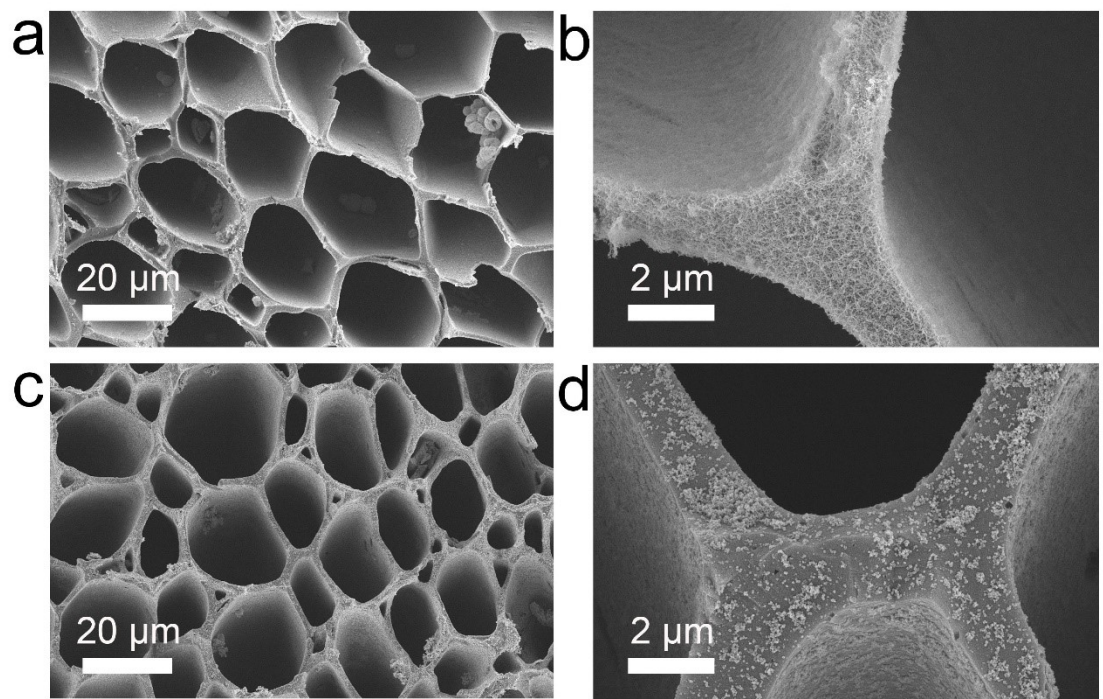


Fig. S3. SEM images of (a, b) Ni-OH@NWC, and (c, d) Ni@NWC.

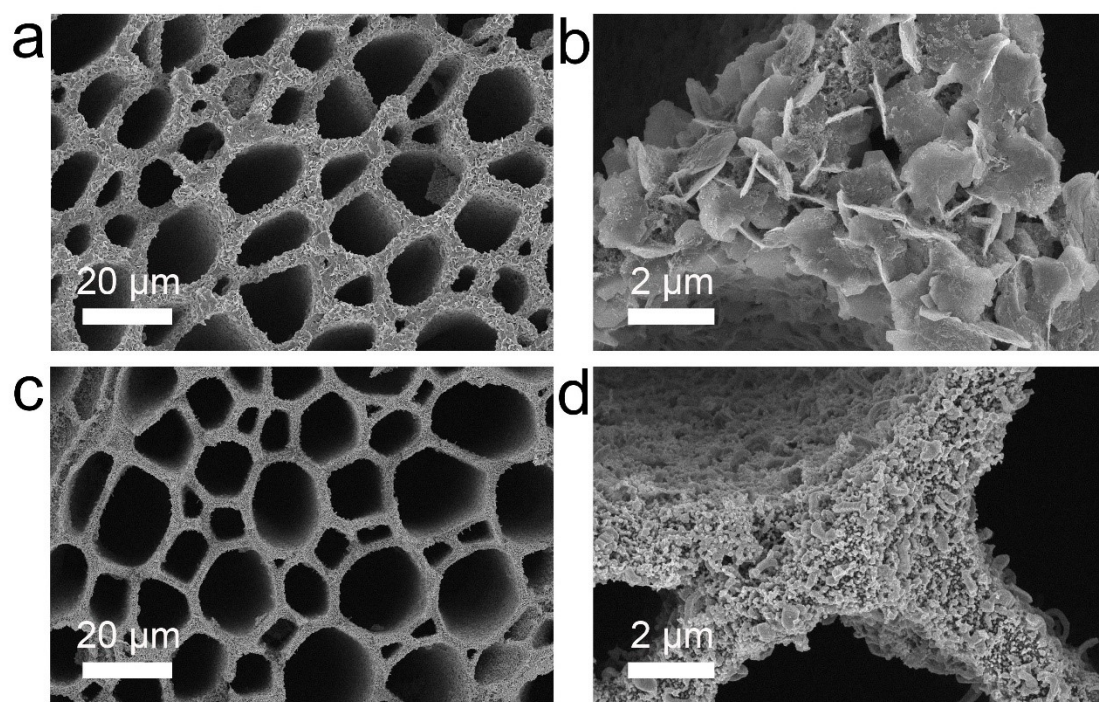


Fig. S4. SEM images of (a, b) FeNi-LDH@NWC, (c, d) FeNi@NWC.

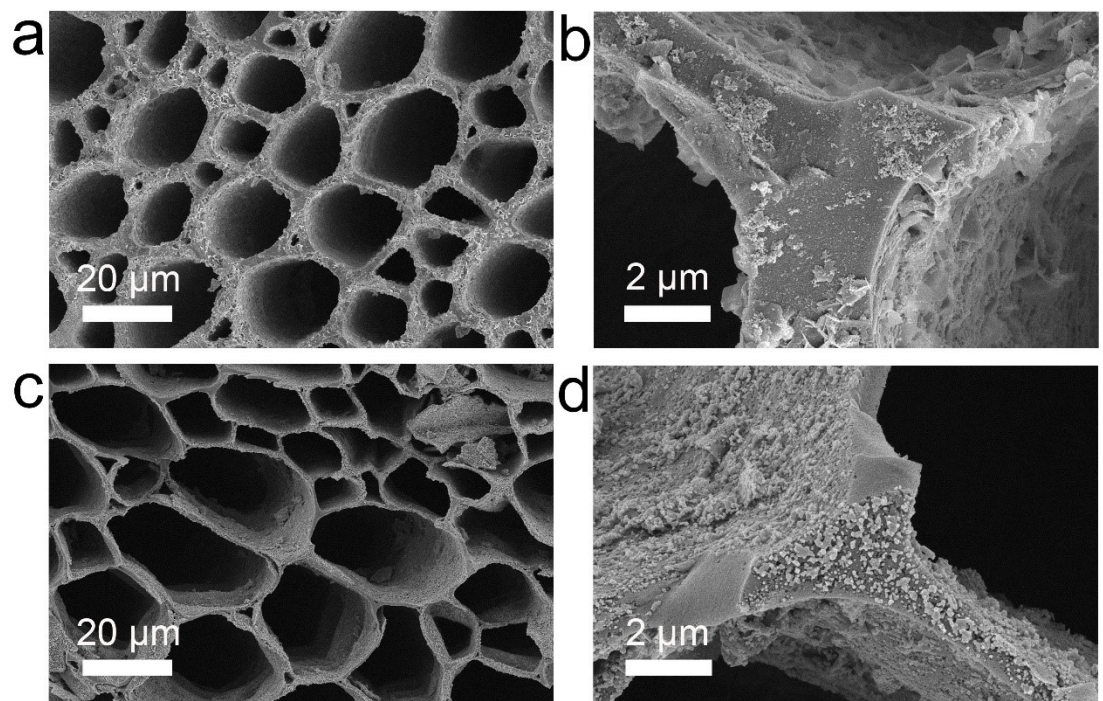


Fig. S5. SEM images of (a, b) $\text{Fe}_3\text{Ni-LDH@NWC}$, and (c, d) $\text{Fe}_3\text{Ni@NWC}$.

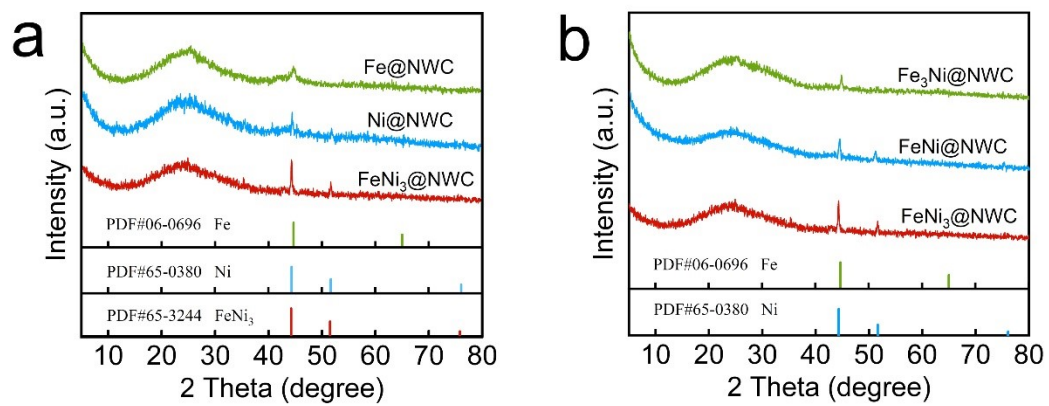


Fig. S6. XRD patterns of some catalysts.

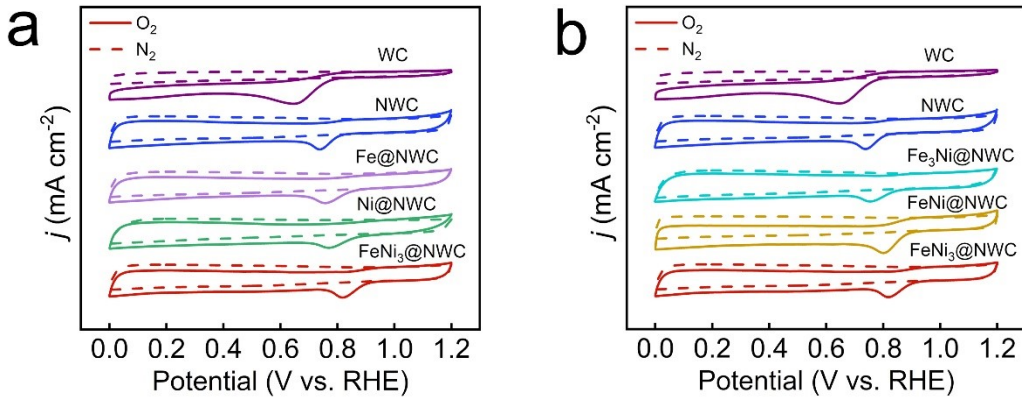


Fig. S7. CV curves of all samples.

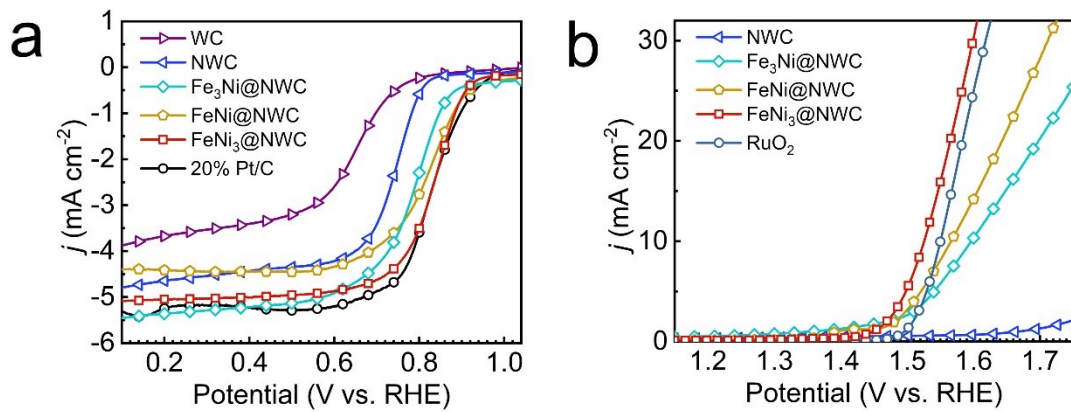


Fig. S8. ORR polarization curves and OER polarization curves of catalysts in different proportions.

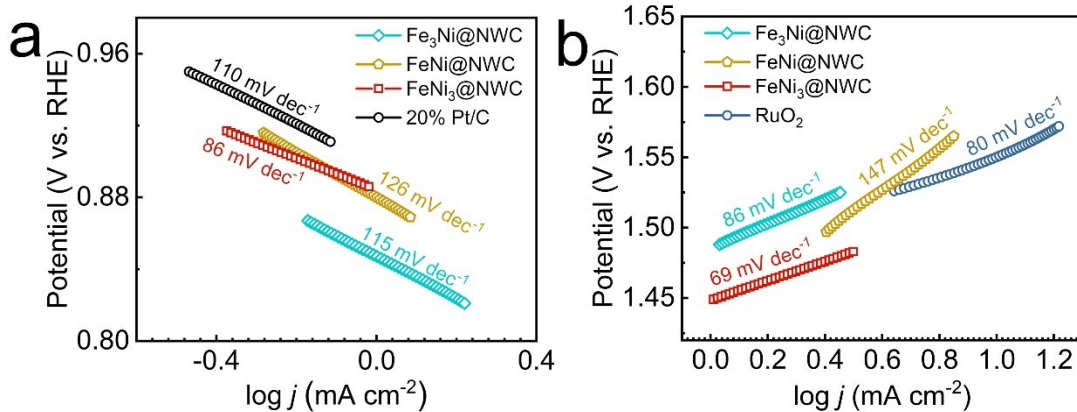


Fig. S9. Tafel plots of (a) ORR, and (b) OER of catalysts.

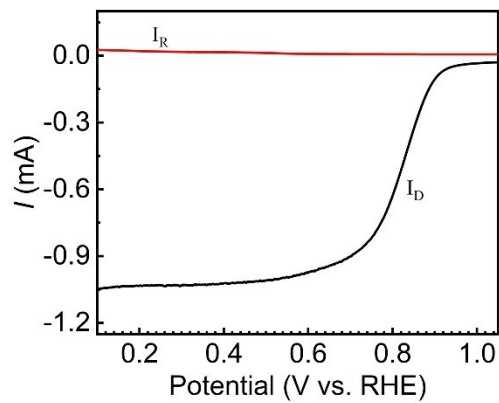


Fig. S10. Disk and ring currents obtained by LSV on a RRDE for FeNi₃@NWC.

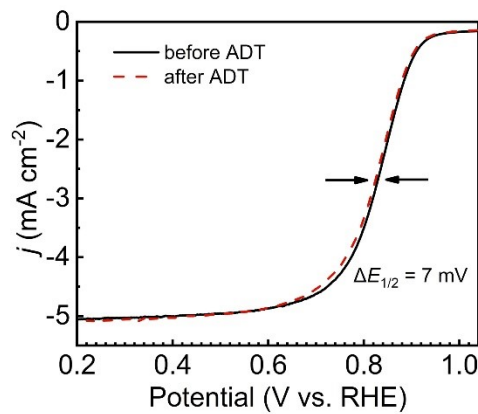


Fig. S11. ORR curves of FeNi₃@NWC before and after ADT.

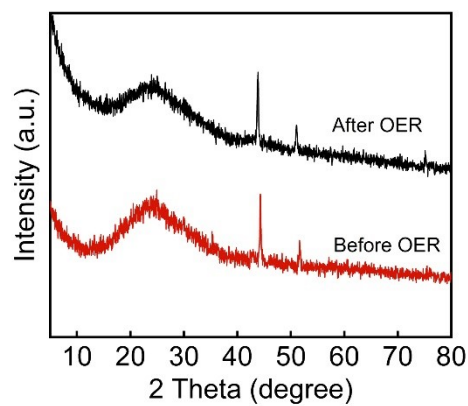


Fig. S12. XRD patterns of $\text{FeNi}_3@\text{NWC}$ before and after OER.

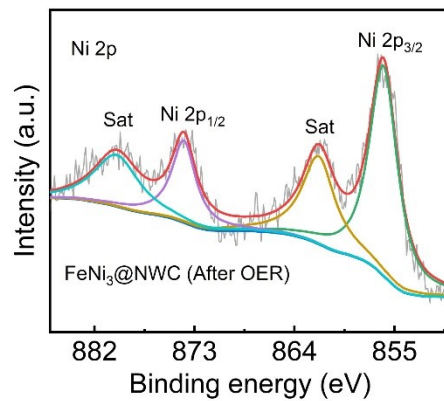


Fig. S13. XPS of Ni 2p for $\text{FeNi}_3@\text{NWC}$ after OER.

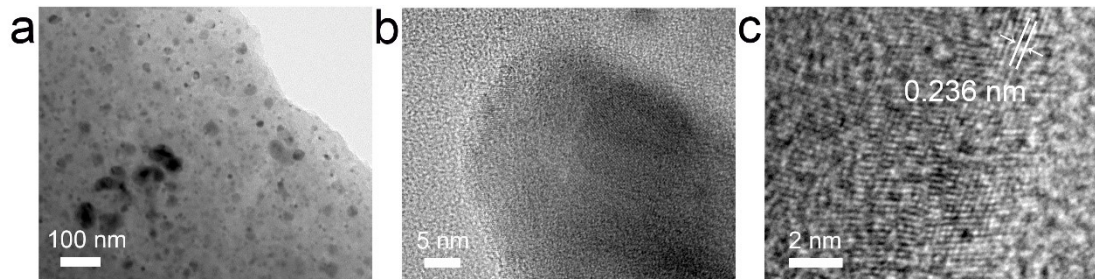


Fig. S14. TEM images of $\text{FeNi}_3@\text{NWC}$ after OER.

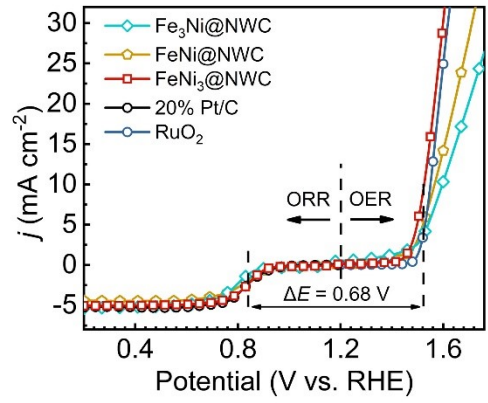


Fig. S15. ORR and OER polarization curves of catalysts in different proportions..

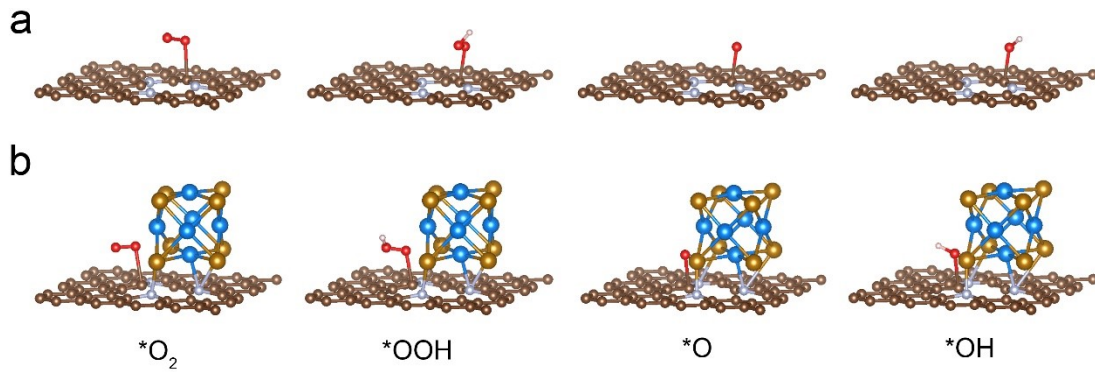


Fig. S16. The configurations for adsorbates ($^*\text{O}_2$, $^*\text{OOH}$, $^*\text{O}$, $^*\text{OH}$) on (a) NC and (b) FeNi₃@NWC in ORR process. Fe, Ni, C, N, O, and H are represented as blue, gold, brown, silver, red, and white spheres, respectively.

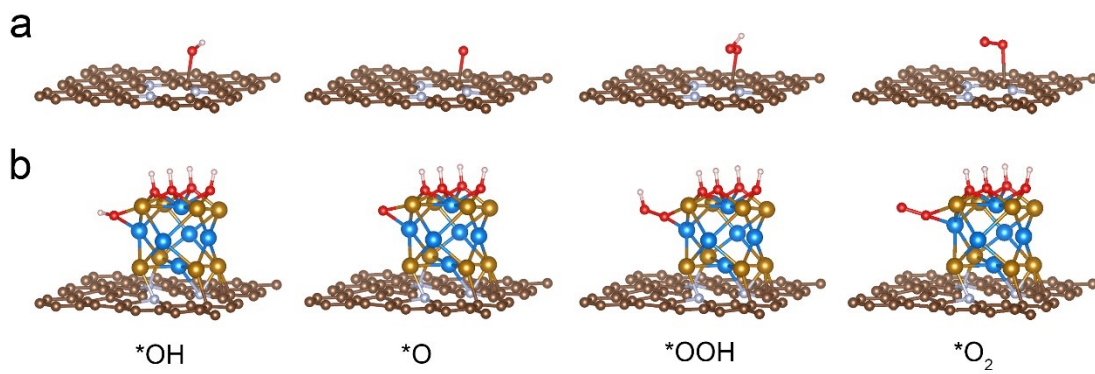


Fig. S17. The configurations for adsorbates ($^*\text{OH}$, $^*\text{O}$, $^*\text{OOH}$, $^*\text{O}_2$) on (a) NC and (b) FeNi₃@NWC in OER process. Fe, Ni, C, N, O, and H are represented as blue, gold, brown, silver, red, and white spheres, respectively.

Table S1. The atomic percentages of FeNi₃@NWC determined by XPS.

	C (at. %)	N (at. %)	O (at. %)	Fe (at. %)	Ni (at. %)
FeNi ₃ @NWC	81.22	4.68	10.23	1.08	2.79

Table S2. Comparison of electrocatalytic ORR and OER activity.

Catalyst	ORR performance		OER performance		ΔE (V)	Reference
	E_{onset} (V)	$E_{1/2}$ (V)	$E_{j=10}$ (mV)	$E_{j=10}$ (V)		
FeNi₃@NWC	0.96	0.84	290	1.52	0.68	This work
CoNP@FeNC-0.05	-	0.85	400	1.63	0.78	S1
FeNi@NCSs	0.93	0.84	318	1.548	0.708	S2
Co _p @CoNC	0.94	0.84	290	1.52	0.68	S3
Fe/Fe ₃ C@N-CNTs	-	0.863	340	1.57	0.707	S4
FeNi/N-LCN	0.975	0.85	340	1.57	0.72	S5
FeNi@NCNT-CP	1	0.85	360	1.59	0.74	S6
Fe,Co,N-C	-	0.90	410	1.64	0.74	S7
Fe-enriched-FeNi ₃ /NC	0.90	0.79	360	1.59	0.80	S8
Fe ₁ Co ₃ -NC-1100	1.05	0.877	349	1.579	0.702	S9
Ni ₃ Fe/N-C	0.92	0.85	330	1.56	0.71	S10

Table S3. Liquid ZABs performance of some previous literature of nonprecious metal.

Catalysts on cathode	Specific capacity (mA h·g _{Zn} ⁻¹)	Durability	Reference
FeNi₃@NWC	805	~266 h (800 cycles) / 5 mA cm⁻²	This work
FeNiP/NPCS	783.5	110 h / 10 mA cm ⁻²	S11
NiFe@C@Co CNFs	694	200 h / 5 mA cm ⁻²	S12
Ni-Fe/Fe ₃ C@NDC	773.8	80 h / 1 mA cm ⁻²	S13
Fe-Co-Ni@NC	754	165 h / 1 mA cm ⁻²	S14
FeCoNC/D	725	40 h / 10 mA cm ⁻²	S15
Fe _{0.5} Co@HOMNCP	786.5	120 h / 2 mA cm ⁻²	S16
CoFe-SNC	636.3	135 h / 10 mA cm ⁻²	S17
Co/Co ₃ O ₄ @CoS-SNC	799	83 h / 5 mA cm ⁻²	S18
Cu ₃ P/MoP@C	704	232 h / 5 mA cm ⁻²	S19
Mo ₂ C/Co@NC	691	180 h / 5 mA cm ⁻²	S20

Table S4. The free energy distribution of water dissociated intermediates on different catalysts.

Catalysts	*H ₂ O (eV)	*OH-H (eV)	*OH+H (eV)
FeNi ₃ @NWC	-0.97584	-0.31547	-1.13569
NWC	-0.54142	0.47514	-0.62251

Table S5. ORR free energy distribution of NWC and FeNi₃@NWC at U = 0 V.

Catalysts	O ₂ (eV)	*OOH (eV)	*O (eV)	*OH (eV)	OH ⁻ (eV)
FeNi ₃ @NWC	4.92	3.78553	2.05432	0.75123	0
NWC	4.92	4.11654	2.11423	0.69266	0

Table S6. ORR free energy distribution of NWC and FeNi₃@NWC at U = 1.23 V.

Catalysts	O ₂ (eV)	*OOH (eV)	*O (eV)	*OH (eV)	OH ⁻ (eV)
FeNi ₃ @NWC	0	0.09553	-0.40568	-0.47877	0
NWC	0	0.42654	-0.34577	-0.53734	0

Table S7. OER free energy distribution of NWC and FeNi₃/(FeNi₃)OOH@NWC at U = 0 V.

Catalysts	OH ⁻ (eV)	*OH (eV)	*O (eV)	*OOH (eV)	O ₂ (eV)
FeNi ₃ /(FeNi ₃)OOH@NWC	0	0.9156	2.24315	3.91536	4.92
NWC	0	0.69266	2.11423	4.11654	4.92

Table S8. OER free energy distribution of NWC and FeNi₃/(FeNi₃)OOH@NWC at U = 1.23 V.

Catalysts	OH ⁻ (eV)	*OH (eV)	*O (eV)	*OOH (eV)	O ₂ (eV)
FeNi ₃ /(FeNi ₃)OOH@NWC	0	-0.3144	-0.21685	0.22536	0
NWC	0	-0.53734	-0.34577	0.42654	0

Reference

1. Y. Y. Xue, Y. B. Guo, Q. M. Zhang, Z. J. Xie, J. P. Wei, Z. Zhou, *Nano-Micro Lett.*, 2022, **14**, 162.
2. S.-Y. Lin, X. Zhang, S.-Y. Sang, L. Zhang, J.-J. Feng, A.-J. Wang, *J. Colloid Interface Sci.*, 2022, **628**, 499-507.
3. H. Yang, S. Gao, D. W. Rao, X. H. Yan, *Energy Stor. Mater.*, 2022, **46**, 553-562.
4. W. W. Xie, T. Z. Tian, M. Yang, N. W. Li, L. Yu, *Appl. Catal. B.*, 2022, **317**, 121760.
5. X. F. Li, Y. J. Liu, H. B. Chen, M. Yang, D. G. Yang, H. M. Li, Z. Q. Lin, *Nano Lett.*, 2021, **21**, 3098-3105.
6. X. J. Zheng, X. C. Cao, K. Zeng, J. Yan, Z. H. Sun, M. H. Rümmeli, R. Z. Yang, *Small*, 2021, **17**, 2006183.
7. S. Sarkar, A. Biswas, E. E. Siddharthan, R. Thapa, R. S. Dey, *ACS Nano*, 2022, **16**, 7890-7903.
8. K. Chen, S. Kim, R. Rajendiran, K. Prabakar, G. Li, Z. C. Shi, C. Jeong, J. Kang, O. L. Li, *J. Colloid Interface Sci.*, 2021, **582**, 977-990.
9. Y. T. He, X. X. Yang, Y. S. Li, L. T. Liu, S. W. Guo, C. Y. Shu, F. Liu, Y. N. Liu, Q. Tan, G. Wu, *ACS Catal.*, 2022, **12**, 1216-1227.
10. H. Y. Gong, X. J. Zheng, K. Zeng, B. Yang, X. Liang, L. Li, Y. Y. Tao, R. Z. Yang, *Carbon*, 2021, **174**, 475-483.
11. J.-T. Ren, Y.-S. Wang, L. Chen, L.-J. Gao, W.-W. Tian, Z.-Y. Yuan, *Chem. Eng. J.*, 2020, **389**, 124408.
12. X. Chen, J. Pu, X. H. Hu, Y. C. Yao, Y. B. Dou, J. J. Jiang, W. J. Zhang, *Small*, 2022, **18**, 2200578.
13. L. Zhang, B. Wang, J. S. Hu, X. H. Huang, W. Y. Ma, N. P. Li, T. Wågberg, G. Z. Hu, *J. Colloid Interface Sci.*, 2022, **625**, 521-531.
14. Y. Ye, L. Zhang, Z. C. Nie, N. P. Li, S. X. Zhou, H. S. Wang, T. Wågberg, G. Z. Hu, *Chem. Eng. J.*, 2022, **446**, 137210.
15. K. Kim, K. Min, Y. Go, Y. Lee, S. E. Shim, D. Lim, S.-H. Baeck, *Appl. Catal. B*, 2022, **315**, 121501.
16. W. Li, B. Liu, D. Liu, P. F. Guo, J. Liu, R. R. Wang, Y. H. Guo, X. Tu, H. G. Pan, D. L. Sun, F. Fang, R. B. Wu, *Adv. Mater.*, 2022, **34**, 2109605.
17. C.-C. Weng, J.-T. Ren, H.-Y. Wang, X.-W. Lv, Y.-J. Song, Y.-S. Wang, L. Chen, W.-W. Tian, Z.-Y. Yuan, *Appl. Catal. B*, 2022, **307**, 121190.

18. H. R. Pan, X. N. Huang, Z. J. Lu, Z. Q. Zhang, B. G. An, D. L. Wu, T. Wang, X. X. Chen, F. Y. Cheng, *Chem. Eng. J.*, 2021, **419**, 129619.
19. M. Guo, M. J. Xu, Y. Qu, C. Hu, P. X. Yan, T. T. Isimjan, X. L. Yang, *Appl. Catal. B*, 2021, **297**, 120415.
20. T. T. Gu, R. J. Sa, L. J. Zhang, D.-S. Li, R. H. Wang, *Appl. Catal. B*, 2021, **296**, 120360.